Submitted to *Geophys. Res. Lett.*: October 14, 1997; Revised December 24, 1997; Accepted January 14, 1998.

Characteristics of magnetic fluctuations within coronal mass ejections: The January 1997 event

Robert J. Leamon, Charles W. Smith and Norman F. Ness

Bartol Research Institute, University of Delaware, Newark

Abstract. We determine the geometry of the fluctuations of the magnetic field at frequencies just above the proton gyrofrequency for the January 10, 1997 CME and the magnetic cloud within. The transverse magnetic fluctuations represent a greater fraction of the magnetic energy than is the case in the typical undisturbed solar wind. The break in the power spectrum that is associated with the the onset of magnetic dissipation falls within the frequency range of interest. The fluctuation geometry is markedly different above and below the spectral break frequency. The inertial range geometry remains unchanged in the cloud with only ~30% of the energy associated with field-aligned wave vectors. The dissipation range wave vectors are highly oblique to the mean magnetic field **B** with up to 96% of the energy associated with oblique wave vectors.

1. Introduction

Studies of the interplanetary magnetic field (IMF) in the undisturbed solar wind have revealed a break in the power spectrum in association with the proton gyrofrequency [*Behannon*, 1976; *Denskat et al.*, 1983; *Smith et al.*, 1990; *Goldstein et al.*, 1994; *Leamon et al.*, 1998]. This spectral break frequency marks the steepening of the power spectrum from the inertial range ($\nu^{-5/3}$) at spacecraft-frame frequencies $10^{-5} \leq \nu_{sc} \leq 0.5$ Hz where the spectral transfer of energy is thought to be energy-conserving to something in the range ν^{-2} to ν^{-4} at $\nu_{sc} \geq 1$ Hz. The association of the spectral break frequency with the proton gyrofrequency Ω_p, together with the analogy drawn from classical turbulence theory [*Batchelor*, 1953], suggests that the onset of dissipation is responsible for the steepening of the spectra, hence our terminology.

A turbulence interpretation would suggest that magnetic dissipation is the ultimate fate for low-frequency magnetic power cascaded from the largest spatial structures. At the same time, fluctuations at $\nu_{sc} \gtrsim \Omega_p/2\pi$ are responsible for scattering low-energy suprathermal particles such as interstellar pickup ions as well as thermal ions and electrons.

Understanding of turbulence and suprathermal particle scattering processes requires determination of the turbulence geometry; i.e., direction of $\mathbf{k}$. The reported observation of magnetic fluctuations perpendicular to the mean magnetic field ($\delta\mathbf{B} \perp \mathbf{B}$) behind high-speed streams [*Belcher and Davis*, 1971] has been used to motivate the slab, or one-dimensional geometry with field-aligned wave vectors, $\mathbf{k}\|\mathbf{B}$. The likelihood that the geometry of the magnetic fluctuations is greater than one-dimensional was shown by *Sari and Valley* [1976]. The possibility that an energetically significant fraction of the wave vectors could reside in a nearly two-dimensional (2D) geometry with both $\mathbf{k} \perp \mathbf{B}$ and $\delta\mathbf{B} \perp \mathbf{B}$ was shown by *Matthaeus et al.* [1990] with further motivation by *Zank and Matthaeus* [1992a]. *Bieber et al.* [1996] assumed the possibility of a composite 2D/slab model for the magnetic turbulence and determined that in the inertial range there is a dominant (~85% by energy) 2D component. The 2D component does not contribute to resonant scattering of very energetic particles (cosmic rays) [*Bieber et al.*, 1994].

Leamon et al. [1998] recently extended the methods of *Bieber et al.* [1996] to the high-frequency end of the inertial range (~0.02 to ~0.2 Hz) and the low-frequency end of the dissipation range (~0.5 to $\lesssim$ 2 Hz) in the undisturbed solar wind. The fluctuations are best characterized by 89% 2D turbulence in the in-

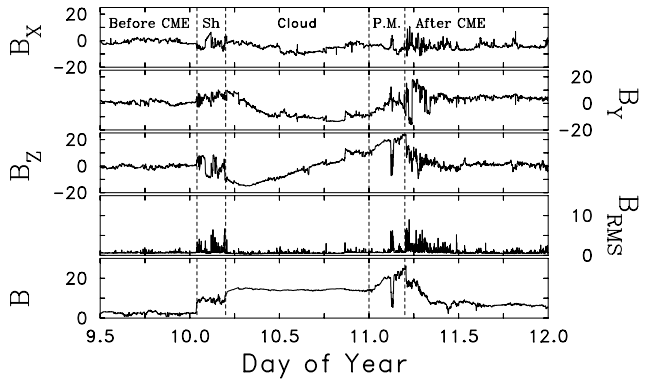

Figure 1. Time series for magnetic field components (B_X, B_Y, B_Z) in nanotesla (nT) and GSE coordinates at 92 second resolution plus magnitude of field and RMS value of fluctuations. Approximate times of non-CME observations, sheath (Sh), cloud, and prominence material (P.M.) as determined by *Burlaga et al.* [1998] are noted in the figure.

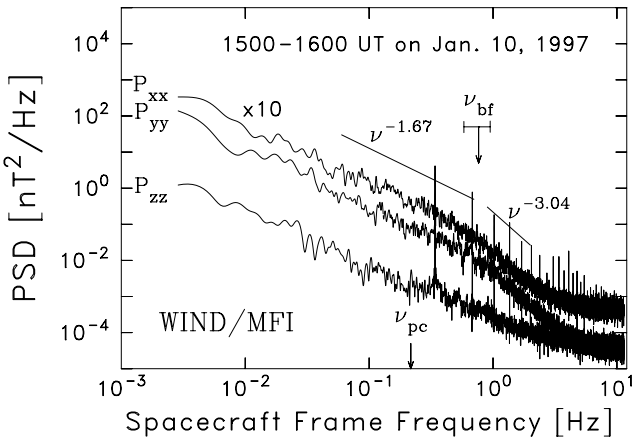

Figure 2. Diagonal elements of power spectral matrix computed in the mean-field coordinate system outlined in the text. Fit spectra for the combined perpendicular components, elevated for clarity, are shown with the fit spectral indexes. The x-component spectrum, P_{xx}, is multiplied by a factor of 10. The other two spectra are shown at computed power levels. Spin tones are evident at multiples of 0.33 Hz and are ignored in this analysis. The break at the dissipation scale (0.77 ± 0.18 Hz) is evident at a frequency greater than the proton gyrofrequency (0.22 Hz). The z component shows significantly less energy than the two perpendicular components until noise dominates the signal at $\nu > 2$ Hz.

ertial range, and 54% 2D turbulence in the dissipation range. The increased slab fraction may be explained by the preferential dissipation of oblique structures. This paper further extends the *Leamon et al.* [1998] analysis by examining observations from within the January 1997 coronal mass ejection (CME) with special emphasis on the embedded magnetic cloud to see how, if at all, the fluctuations within a CME differ from those in the undisturbed solar wind.

2. Observations

Figure 1 shows the magnetic field data from the WIND/MFI experiment [*Lepping et al.*, 1995] for the $2\frac{1}{2}$-day interval from January 9, 1200 UT (DOY 9.5) to January 12, 0000 UT (DOY 12.0) that contains the CME. We divide this interval into 5 distinct regions: the solar wind prior to the CME (prior to the shock at DOY 10.0); the sheath region between the shock and the beginning of the cloud at DOY 10.2; the magnetic cloud, which we have taken to end at DOY 11.0, when B starts to increase above 14 nT; the solar prominence material at the beginning of January 11; and the solar wind behind the CME (after DOY 11.2). For more detailed analyses of the CME structure, the cloud and the identification of the solar prominence material, see *Burlaga et al.* [1998]. Not shown in Figure 1 are the plasma data, which show that the solar wind speed V_{SW} is very low prior to the CME and high following the CME; and that V_{SW}, the proton temperature and proton density are all extremely constant within the magnetic cloud.

We have divided the 60-hour interval shown in Figure 1 into 60 1-hour subintervals and we have analysed the spectral properties for each subinterval in the range of spacecraft-frame frequencies $0.02 \lesssim \nu_{sc} \lesssim 0.2$ Hz, which is the high-frequency end of the inertial range, and the range $1 < \nu_{sc} < 2$ Hz, which is the low-frequency end of the dissipation range. Figure 2 shows the spectrum for one subinterval within the magnetic cloud. The data are rotated into a right-handed orthogonal mean-field coordinate system: the z axis is aligned with the mean magnetic field and points away from the Sun; the x axis is in the plane defined by the mean field $\hat{\mathbf{B}}$ and the radial vector $\hat{\mathbf{R}}$ and also points away from the sun; the y axis completes the right-handed system. This is the $(\hat{\mathbf{x}}, \hat{\mathbf{y}}, \hat{\mathbf{z}})$ system used by *Bieber et al.* [1996].

We used a pre-whitened correlation function method [*Blackman and Tukey*, 1958] to compute the magnetic power spectrum of each subinterval. The inertial and

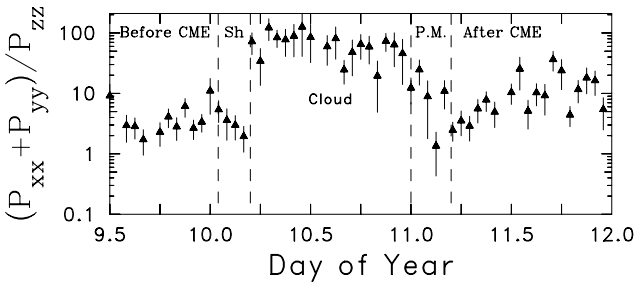

Figure 3. Ratio of transverse to field-aligned power in the inertial-range spectrum of magnetic fluctuations for each of the 60 hourly subintervals. Uncertainties are computed from the variation of the power ratio computed across the frequency interval. The anisotropy of the dissipation-range fluctuations could not be computed due to the noise level in the P_{zz} component.

dissipation ranges of each interval's spectrum are fitted with power laws and the frequency at which the break occurs is computed from the intersection of the two power laws. Figure 2 shows sharp peaks at harmonics of the spacecraft spin-tone; these are an almost omni-present feature in the spectra. These are thought to result from thermal currents near the sensors. Consequently, these frequencies (harmonics of 0.33 Hz) are omitted from the least-squares fitting of the two ranges using a $\pm 10\%$ window around each harmonic.

The other feature of Figure 2 is the flattening of the spectrum at high frequencies. This is not a feature of the interplanetary turbulence and remains a subject of examination by the WIND MFI team. The intrinsic noise levels for the triaxial fluxgate magnetometer, including digitization error, is a factor of 3–5 lower than observed here [*Lepping et al.*, 1995]. We exclude the contaminated frequencies from this analysis.

3. Anisotropy

In a classic study of the undisturbed solar wind, for the frequency range $1.6 \times 10^{-4} \leq \nu_{sc} \leq 0.04$ Hz, *Belcher and Davis* [1971] showed that there was a 9:1 anisotropy between average variances transverse and parallel to the mean magnetic field. *Leamon et al.* [1998] used the ratio between spectral powers and obtained broadly similar results for the high-frequency extension of the inertial range, where the anisotropy in the inertial range was 10.4:1, which decreased to 4.9:1 in the dissipation range.

Repeating the *Leamon et al.* analysis yields inertial range anisotropies less than *Belcher and Davis* before the magnetic cloud in the solar wind: the transverse-to-parallel ratio is $(3.4 \pm 0.5) : 1$. In the sheath region, where the fluctuation levels (B_{rms}) are elevated, the fluctuation anisotropy does not change significantly and the ratio is $(4.2 \pm 1.5) : 1$. In the magnetic cloud, however, the fluctuations are highly transverse: within the cloud the ratio is $(61.7 \pm 8.5) : 1$. Figure 3 shows the inertial-range anisotropy ratio for each hour-long subinterval through the whole event. The magnetic cloud, as defined by *Burlaga et al.* [1998] and shown in Figure 1, is clearly identifiable from the enhanced transverse power.

In the high speed solar wind behind the magnetic cloud the anisotropy ratio is not steady, but is more consistent with the conclusions of *Belcher and Davis* [1971] at $(8.2 \pm 1.3) : 1$. It is hard to differentiate the prominence material from the high speed solar wind from the anisotropy results and Figure 3 alone.

The transverse nature of the fluctuations within the CME and cloud would seem to suggest the applicability of scattering theories employing the slab approximation [see, e.g., *Jokipii*, 1966], but we see in the next section that the slab approximation is inappropriate.

4. Geometry

The *Belcher and Davis* anisotropy is consistent with 2D, even though it is sometimes taken as evidence of slab waves. By 2D turbulence we mean fluctuations that have wave vectors that are nearly transverse to the mean magnetic field. The mean-field coordinate system outlined in section 2 was specifically chosen because the ratio of transverse spectral powers P_{yy}/P_{xx} gives a direct link to the percentage of slab and 2D fluctuations [*Oughton*, 1993; *Bieber et al.*, 1996].

We assume that the magnetic fluctuations consist of a mixture of slab (with $\mathbf{k} \| \mathbf{B}$) and 2D (with $\mathbf{k} \perp \mathbf{B}$) geometries and compute their relative strengths from the ratio of transverse spectral powers.

C_S and C_2 are the amplitudes of the slab and 2D components of the energy spectrum [*Bieber et al.*, 1996]. We further assume that the two components obey the same power law (same spectral index $-q$). Thus, the slab spectrum in the range of interest is parameterized by $C_S \nu^{-q}$ and the 2D spectrum by $C_2 \nu^{-q}$.

The "slab fraction" r is the ratio of the slab com-

ponent of the energy spectrum to the total energy:

$$r \equiv \frac{C_S}{C_S + C_2} = \frac{1}{1 + r'}, \qquad (1)$$

where $r' = C_2/C_S$. Equations (16) and (17) of *Bieber et al.* [1996] and the above definition leads to the following formula for the ratio of power between components:

$$\frac{P_{yy}(\nu)}{P_{xx}(\nu)} = \frac{\left(\frac{2\pi}{V_{SW}\cos\theta}\right)^{1-q} + r'\frac{2q}{1+q}\left(\frac{2\pi}{V_{SW}\sin\theta}\right)^{1-q}}{\left(\frac{2\pi}{V_{SW}\cos\theta}\right)^{1-q} + r'\frac{2}{1+q}\left(\frac{2\pi}{V_{SW}\sin\theta}\right)^{1-q}} \qquad (2)$$

The ratio P_{yy}/P_{xx} (which under our assumptions becomes independent of frequency in the relevant range) and the parameters V_{SW}, $\theta = \Theta_{BV}$, the angle between the magnetic field and solar wind velocity, and q are derivable from observations by a single spacecraft. Thus the only unknown in equation (2) is r', which, in turn, gives us the slab fraction r.

For both slab and 2D models, there is no power in the parallel fluctuations and $P_{zz}(\nu) = 0$. That P_{zz} is ~70 times smaller than $P_{yy} + P_{xx}$, as discussed in section 3, is a good approximation to this. Furthermore, for pure slab turbulence ($r = 1$; $r' = 0$) axisymmetry leads to equality of P_{xx} and P_{yy} [*Bieber et al.*, 1996]. Pure 2D turbulence predicts that the ratio $P_{yy}(\nu)/P_{xx}(\nu)$ be equal to the power law index q.

The results of P_{yy}/P_{xx} as a function of Θ_{BV} for the magnetic cloud are shown in Figure 4; the solid curves through the data represent minimum χ^2 values of r, assuming a constant (average) value of spectral index q. Although the curves shown use the average value of the spectral indices, the χ^2 statistics of the fit were evaluated using observed values of q of each individual subinterval (dashed lines). For the high-frequency end of the inertial range (upper panel of Figure 4) the minimum χ^2 of 7.90 occurs at $r = 0.29 \pm 0.29$. For the dissipation range (lower panel of Figure 4) the minimum χ^2 of 1.35 occurs at $r = 0.04^{+0.25}_{-0.04}$. The indicated error bounds were determined from the values of r for which $\chi^2(r) = \chi^2_{\rm min} + 1$ [*Bevington*, 1969].

In the undisturbed solar wind [*Leamon et al.*, 1998] the inertial range consists of 89% 2D turbulence and 11% slab waves and the dissipation range consists of 54% 2D turbulence and 46% slab waves. In *Leamon et al.* [1998], we postulate that the increased dissipation range slab fraction is due to preferential dissipation of 2D structures. This assumption is inadequate in the magnetic cloud, where the slab waves are completely absent. At the same time, we must reconcile the *increased* inertial range slab fraction (29% compared to

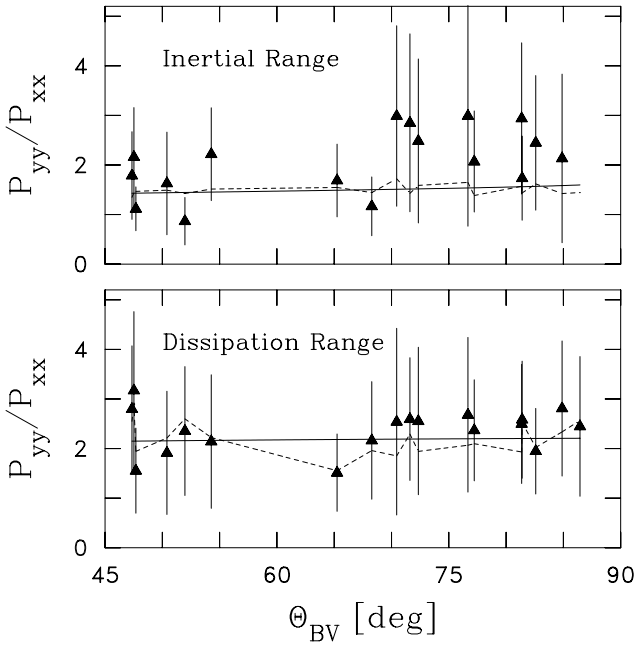

Figure 4. Geometry of the magnetic fluctuations in the high frequency region of the inertial range (top panel) and the dissipation range (bottom panel). In both cases the energy is composed predominantly, and almost exclusively, by 2D fluctuations with wave vectors nearly at right angles to the ambient magnetic field. The solid curves correspond to the best-fit values of r using the average spectral index: for the inertial range, $r = 0.29$, and for the dissipation range $r = 0.04$. The dashed lines correspond to the best-fit values using the individual observed spectral indices. Uncertainties are computed from the variation of the power ratio computed over the spectral subrange in question.

11%) in the magnetic cloud. Within error bounds, the inertial range values are the same.

We repeat the geometry fitting analysis for the slow solar wind prior to the CME and in the high speed stream that follows it. In the 12 hours prior to the shock, the inertial range is also best described by 29% slab waves ($r = 0.29^{+0.31}_{-0.22}$ with $\chi^2_{\rm min} = 1.63$); however, the dissipation range is 91% slab waves ($r = 0.91^{+0.08}_{-0.16}$ with $\chi^2_{\rm min} = 4.87$). In the high-speed stream the inertial range is best characterized by a 34% slab component ($r = 0.34^{+0.25}_{-0.23}$ with $\chi^2_{\rm min} = 4.88$), and the dissipation range by $r = 0.32^{+0.13}_{-0.11}$ ($\chi^2_{\rm min} = 2.64$).

If we explain the increase of one geometry in the

dissipation range of the spectrum to be due to the preferential dissipation of the other, why is the cloud's geometry almost purely 2D fluctuations while in the preceding solar wind, the fluctuations are over 90% Alfvénic? The inertial range geometry is approximately constant at 30% slab waves; it is the dissipation range geometry that varies. From the preceding solar wind to the high-speed stream to the cloud, the average proton plasma β decreases from 1.362 to 0.609 to 0.039, and the proportion of slab waves decreases from 91% to 32% to 4%. Low β favors the collapse to 2D, as is suggested by considering the equations of reduced MHD [*Zank and Matthaeus*, 1992b], and this process may be more rapid at the smaller scales of the dissipation range.

We tried to fit geometry models to the sheath and prominence observations, but the uncertainties and χ^2 values were too large to lend confidence to the results.

5. Conclusions

We have shown that magnetic fluctuations in the cloud are even more transverse than in the highly Alfvénic, undisturbed solar wind (68:1 as compared with 9:1). Analysis of the geometry of the high-frequency, transverse fluctuations within the cloud reveal that at dissipation range frequencies the energy resides almost entirely within a two-dimensional geometry with wave vectors normal to the mean field direction. Outside the cloud the fluctuation geometries are more slab-like, a fact that may be reconciled with the sharply reduced values of β inside the magnetic cloud.

Regardless of whether the 2D component is dynamical turbulence, waves or static structures, attempts to describe energetic charged particle scattering within the CME must consider the reduced availability of energy in the slab component that lowers scattering efficiencies by the ratio of slab to total magnetic power. The possibility remains that the 2D component could produce significant scattering of low-energy charged particles.

Acknowledgments. This work is supported by the WIND mission through NASA subcontract NAG5-2848 to the Bartol Research Institute. The authors wish to thank the P.I. of the WIND Magnetic Field Experiment, R.P. Lepping, for making the data available for this study. We also wish to acknowledge helpful conversations with W.H. Matthaeus and M.L. Goldstein.

References

Batchelor, G. K., *The Theory of Homogeneous Turbulence*, Cambridge University Press, New York, 1953.

Behannon, K. W., Observations of the Interplanetary Magnetic Field Between 0.46 and 1 AU by the Mariner 10 Spacecraft, Ph.D. Thesis, Catholic University of America, Washington DC, 1975.

Belcher, J. W., and L. Davis, Jr., Large-amplitude Alfvén waves in the interplanetary medium, 2, *J. Geophys. Res.*, *76*, 3533–3563, 1971.

Bevington, P. R., *Data Reduction and Error Analysis for the Physical Sciences*, McGraw-Hill, New York, 1969.

Bieber, J. W., W. H. Matthaeus, C. W. Smith, W. Wanner, M.-B. Kallenrode, and G. Wibberenz, Proton and electron mean free paths: The Palmer consensus revisited, *Astrophys. J.*, *420*, 294–306, 1994.

Bieber, J. W., W. Wanner, and W. H. Matthaeus, Dominant two-dimensional solar wind turbulence with implications for cosmic ray transport, *J. Geophys. Res.*, *101*, 2511–2522, 1996.

Blackman, R. B., and J. W. Tukey, *The Measurement of Power Spectra*, Dover, New York, 1958.

Burlaga, L. F., *et al.*, A magnetic cloud containing prominence material: January 1997, *J. Geophys. Res.*, *103*, 277–286 1998.

Denskat, K. U., H. J. Beinroth and F. M. Neubauer, Interplanetary magnetic field power spectra with frequencies from 2.4×10^{-5} Hz to 470 Hz from Helios-observations during solar minimum conditions, *J. Geophys.*, *54*, 60–67, 1983.

Goldstein, M. L., D. A. Roberts and C. A. Fitch, Properties of the fluctuating magnetic helicity in the inertial and dissipation ranges of solar wind turbulence, *J. Geophys. Res.*, *99*, 11 519–11 538, 1994.

Jokipii, J. R., Cosmic-ray propagation. I. Charged particles in a random magnetic field, *Astrophys. J.*, *146*, 480–487, 1966.

Leamon, R. J., C. W. Smith, N. F. Ness, W. H. Matthaeus and H. K. Wong, Observational constraints on the dynamics of the interplanetary magnetic field dissipation range, *J. Geophys. Res.*, in press, 1998.

Lepping, R. P., *et al.*, The WIND magnetic field investigation, *Space Science Reviews*, *71*, 207–229, 1995.

Matthaeus, W. H., M. L. Goldstein, and D. A. Roberts, Evidence for the presence of quasi-two-dimensional nearly incompressible fluctuations in the solar wind, *J. Geophys. Res.*, *95*, 20 673–20 683, 1990.

Oughton, S., Transport of Solar Wind Fluctuations: A Turbulence Approach, Ph.D. Thesis, Univ. of Del., Newark, 1993.

Sari, J. W., and G. C. Valley, Interplanetary magnetic field power spectra: Mean field radial or perpendicular to radial, *J. Geophys. Res.*, *81*, 5489–5499, 1976.

Smith, C. W., W. H. Matthaeus, and N. F. Ness, Measurement of the dissipation range spectrum of magnetic fluctuations in the solar wind with applications to the

diffusion of cosmic rays, *Proc.* $21^{\underline{st}}$ *Internat. Cosmic Ray Conf.* (Adelaide), *5*, 280–283, 1990.

Zank, G. P., and W. H. Matthaeus, Waves and turbulence in the solar wind, *J. Geophys. Res.*, *97*, 17 189–17 194, 1992a.

Zank, G. P., and W. H. Matthaeus, The Equations of Reduced Magnetohydrodynamics, *J. Plasma Phys.*, *48*, 85–100, 1992b.

R.J. Leamon, C.W. Smith, N.F. Ness, Bartol Research Institute, University of Delaware, Newark, DE 19716.
(e-mail: leamon@bartol.udel.edu, nfness@bartol.udel.edu, and chuck@bartol.udel.edu)

October 14, 1997; revised December 24, 1997; accepted January 14, 1998.

This preprint was prepared with AGU's LaTeX macros v4. File CMEDISS formatted January 21, 1998.

With the extension package 'AGU^{++}', version 1.2 from 1995/01/12